GEOPHYSICS, VOL. 88, NO. 2 (MARCH-APRIL 2023); P. M105–M117, 16 FIGS., 4 TABLES.
10.1190/GEO2022-0352.1

# Iterative geostatistical seismic inversion with rock-physics constraints for permeability prediction

Roberto Miele[1], Dario Grana[2], Luiz Eduardo Seabra Varella[3], Bernardo Viola Barreto[3], and Leonardo Azevedo[1]

## ABSTRACT

Accurate prediction of the spatial distribution of subsurface permeability is a fundamental task in reservoir characterization and monitoring studies for hydrocarbon production and $CO_2$ geologic storage. Predicting permeability over large areas is challenging, due to their high variability and spatial anisotropy. Common approaches for modeling permeability generally involve deterministic calculations from porosity using precalibrated rock-physics models (RPMs) or geostatistical cosimulation methods that reproduce observed experimental porosity-permeability relationships. Instead, we have predicted permeability from seismic data using an iterative geostatistical seismic inversion method that combines the advantages of rock-physics and geostatistical modeling methods. First, we simulate facies through 1D vertical Markov chain simulations. Then, permeability, porosity, and acoustic impedance are sequentially generated and conditioned to the previously simulated facies model. An RPM is used to evaluate the misfit between the permeability predictions obtained from geostatistical cosimulation at the well locations and well-log values computed from the acoustic impedance. The residuals of the misfit function are used as conditioning constraints in the stochastic update of the models in the subsequent iteration. The outcome of our methodology is a set of multiple geostatistical realizations of facies, permeability, porosity, and acoustic impedance conditioned to seismic data and constrained by an RPM. We first illustrate the method on a synthetic 1D example and compare it to a traditional geostatistical inversion approach. We then apply our inversion to a 3D real data set to assess the methodology performance with scarce conditioning data and in the presence of noise.

## INTRODUCTION

The permeability of porous rocks is a physical property that defines the ability of a given fluid to flow through the pore space. In reservoir characterization, accurate predictions of the spatial distribution of permeability are fundamental to optimize production and well placement in hydrocarbon exploration and to monitor the migration of the $CO_2$ plume in carbon geologic storage. Absolute permeability describes the permeability of a rock fully saturated with a single fluid phase (e.g., water); in the presence of two or more saturating fluids, the effective permeability defines the permeability of one fluid (e.g., water, oil, or gas) with respect to the others. The ratio between effective and absolute permeability is defined as the relative permeability (e.g., Yang, 2017). In this work, we use the term permeability to indicate absolute permeability.

The spatial variability of rock permeability depends on rock sedimentary and tectonic evolution and their texture and structure. Even within the same rock type or lithofluid facies, permeability values vary over several orders of magnitude, generally defining a positive skewed distribution. A detailed discussion on this topic can be found, for example, in Shepherd (1989), Nelson (1994), Yang (2017), and Ma (2019). The investigation of permeability accounts for direct and indirect measuring techniques. Permeability can be directly measured on core samples (e.g., Lishman, 1970; Butler, 2005; Yang, 2017). Alternatively, permeability can be estimated from nuclear magnetic resonance well logs, according to relationships linking the transverse

Manuscript received by the Editor 7 June 2022; revised manuscript received 22 September 2022; published ahead of production 2 January 2023; published online 27 March 2023.
[1]Universidade de Lisboa, CERENA, DER, Instituto Superior Técnico, Lisboa, Portugal. E-mail: roberto.miele@tecnico.ulisboa.pt (corresponding author); leonardo.azevedo@tecnico.ulisboa.pt.
[2]University of Wyoming, Department of Geology and Geophysics, School of Energy Resources, Laramie, Wyoming, USA. E-mail: dgrana@uwyo.edu.
[3]PETROBRAS — EXP/GEO/TGEO, Rio de Janeiro, Brazil. E-mail: luizedu@petrobras.com.br; bernardo.barreto@petrobras.com.br.

relaxation time constant ($T_2$) to pores characteristics (Coates et al., 1999; Dunn et al., 2002; Ellis and Singer, 2007; Lee and Waite, 2008) or Stoneley waves well logs, based on the induced fluid flow (Ellis and Singer, 2007; Silva et al., 2019).

The effect of permeability variations on elastic and seismic properties has been studied in poroelasticity theory (Biot, 1956a, 1956b; Carcione, 2015). As first theorized by Biot (1956a, 1956b) and later expanded by White et al. (1975) and Dvorkin et al. (1994), a wave-induced flow of the rock-saturating fluids causes an attenuation that depends on the rock permeability. The relation between permeability and seismic attenuation has been studied by Shapiro and Müller (1999), Pride et al. (2003, 2004), Goloshubin et al. (2008), Rubino et al. (2012), and Iturrarán-Viveros and Parra (2014). Permeability also can be estimated from seismic monitoring surveys and production data in time-lapse seismic inversion and seismic history-matching studies (Landrø, 2001; Vasco et al., 2004; Dadashpour, 2009; Dadashpour et al., 2010; Feng and Mannseth, 2010); however, this approach requires time-lapse seismic data and can only be applied in the production phase.

Predicting rock and fluid properties from seismic data is an inverse problem where the optimal solution ($\hat{\mathbf{m}}$) is the solution of a minimization problem of the form

$$\hat{\mathbf{m}} = \arg\min \|\mathbf{d}_{\text{obs}} - \mathbf{F}(\mathbf{m})\|, \tag{1}$$

where $\mathbf{m}$ represents the model parameters, $\mathbf{d}_{\text{obs}}$ represents the observed seismic data, and $\mathbf{F}$ is a nonlinear geophysical function based on seismic wavefield propagation, poroelasticity, or geomechanics. Examples of inverse problems for reservoir characterization include seismic inversion (Tarantola, 2005) and petrophysical inversion (Doyen, 2007; Bosch et al., 2010; Grana et al., 2021). Seismic and petrophysical inversion methods can be broadly divided into deterministic and statistical methods (Bosch et al., 2010; Grana et al., 2021). Statistical methods include Bayesian linearized seismic and petrophysical inversion (e.g., Buland and Omre, 2003; Grana and Della Rossa, 2010) and stochastic sampling and optimization (de Figueiredo et al., 2018; Fjeldstad and Omre, 2020). Stochastic optimization methods can be combined with geostatistical simulations and geophysical inversion to generate high-resolution models and update them according to the measured geophysical data (e.g., Deutsch and Journel, 1997; Deutsch, 2002; Dubrule, 2003; Doyen, 2007; Soares et al., 2007; González et al., 2008; Grana et al., 2012; Azevedo et al., 2020b).

A detailed description of the relationship between petrophysical and elastic properties can be found in Avseth et al. (2005), Ellis and Singer (2007), Dvorkin et al. (2014), Mavko et al. (2019), and Grana et al. (2021). An extensive analysis of the relationship between porosity and permeability is given by Nelson (1994). Porosity-permeability relations include empirical and physics-derived rock-physics equations based on the Kozeny-Carman relation and RPGZ equation (Kozeny, 1927; Carman, 1937; Mavko and Nur, 1997; Glover et al., 2006; Mavko et al., 2019). These models require the knowledge of specific rock parameters (e.g., pore shapes or cementation) that might differ from one facies to another and must be calibrated with experimental data (i.e., well-logs or core samples). These relations can be integrated in seismic inversion workflows (e.g., Tiab and Donaldson, 2012; Ma, 2019), but might fail to reproduce the spatial variability of permeability.

Alternatively, permeability can be predicted from porosity models using geostatistical methods (Deutsch and Journel, 1997), for example, using stochastic sequential cosimulation that reproduces the joint distribution of permeability and porosity (e.g., Horta and Soares, 2010). These methods rely on the experimental distribution observed at the well locations, but generally, they do not include physics-based constraints and might lead to geologically implausible predictions.

The main goal of this work is to combine rock-physics relations and geostatistical methods to predict permeability from seismic data in an iterative geostatistical seismic inversion approach based on stochastic sequential simulation and cosimulation. Sequential simulations (e.g., Soares, 2001; Horta and Soares, 2010) reproduce the joint distributions of porosity and permeability and their spatial correlations (i.e., variogram model), whereas the rock-physics model (RPM) introduces a physical constraint. The proposed seismic inversion algorithm is applied to discrete (i.e., lithofluid facies) and continuous (i.e., permeability, porosity, and acoustic impedances) properties and is applied to poststack seismic data. However, the inversion can be extended to prestack seismic data and various model parameterizations. The methodology is demonstrated with synthetic and real data and the results are compared with an iterative geostatistical seismic inversion methodology for validation.

## METHODOLOGY

We propose an iterative geostatistical seismic inversion method for the prediction of subsurface permeability distribution. The algorithm is based on stochastic perturbation optimization for discrete-continuous inverse problems (Azevedo et al., 2020a) and integrates rock-physics and seismic data constraints in its objective function. Each step of the algorithm is illustrated in Figure 1 and described next.

A set of $N$ facies models is initially simulated, sampling from a first-order Markov chain distribution. A set of $N$ models of permeability, porosity, and acoustic impedance is simulated subsequently, using direct sequential simulation (DSS) and cosimulation (co-DSS), according to the prior distribution and the prior variogram model (Soares, 2001; Horta and Soares, 2010), conditioned on the facies realizations (Nunes et al., 2017). The acoustic impedance models are used to compute $N$ synthetic seismic models by calculating the convolution of a known wavelet with the reflectivity coefficients. The seismic models are compared with real seismic data to assess the similarity of the predictions with the observed data. At the same time, the acoustic impedance models are used to compute a secondary set of permeability models, using precalibrated and facies-dependent RPMs. Such permeability models represent the expected permeability given the distribution of elastic rock properties and their correlation with the acoustic properties. The rock-physics-derived permeability models are compared locally to the geostatistically simulated permeability realizations and their similarity is computed to quantify the coherency between the geostatistical simulations and the rock-physics predictions (Figure 2). The two similarities coefficients are combined through a weighted average at each cell of the inversion grid to determine the realization with the highest (combined) similarity. At the end of each iteration, the realizations that have the highest similarity coefficients are used to condition the simulation of a new set of geostatistical realizations in the subsequent iteration.

## Facies simulations

We assume that the facies distribution follows a first-order hidden Markov chain model along a vertical direction (Krumbein and Dacey, 1969; Elfeki and Dekking, 2001; Lindberg and Omre, 2015; Fjeldstad and Omre, 2020). This means that the facies occurrence at a given location is conditioned exclusively by the facies simulated at the location immediately above. The transition probabilities $P_{i,j}$ are defined in a vertical transition matrix, where each row represents the facies at the location above and the columns represent the facies at the current location where the facies simulation is being performed. The transition matrix is generally inferred from the facies-log data.

To generate geostatistical realizations of facies, at each trace location, we draw a random value at the first sample of the inversion grid directly from a prior distribution $P(\mathbf{f})$ representing the prior facies proportions. Then, we subsequently simulate the following samples along the vertical direction from the transition probabilities:

$$P_{i,j} = P(\mathbf{f}_t = i | \mathbf{f}_{t-1} = j), \qquad (2)$$

where $i$ and $j = 1, \ldots, N_f$ ($N_f$ being the number of facies) and $t = 2, \ldots, N_s$ ($N_s$ being the number of samples of the seismic trace). The simulation is sequentially performed at all trace locations within the inversion grid. At each iteration $l$ of the stochastic method, we obtain a set of $N_r$ realizations of facies models that we denote with $\mathbf{f}^{l,r}$.

## Petroelastic properties simulations

The simulated facies models are used as conditioning data for the generation of petrophysical models of permeability ($\mathbf{k}$) and porosity ($\boldsymbol{\phi}$) and elastic models of acoustic impedance ($\mathbf{I_P}$) using DSS and co-DSS (Soares, 2001; Horta and Soares, 2010). As we are basing our method in a geostatistical framework, we first generate the property that is less related to the seismic data (i.e., more uncertain) so it explores more widely the model parameter space. The same approach is followed, for example, in geostatistical seismic amplitude variation with angle inversion (e.g., Azevedo et al., 2019). Simulating permeability from porosity would limit the range of solutions explored: the iterative convergence towards the desired solution would be driven by porosity. We locally condition the petroelastic simulations on the facies models using multilocal distribution functions (Nunes et al., 2017). DSS and co-DSS reproduce prior marginal and joint distributions of $\mathbf{k}$, $\boldsymbol{\phi}$, and $\mathbf{I_P}$ and corresponding variograms estimated from the existing well-log data. At a given iteration $l$ and for every set of realizations $r$, we first simulate permeability using DSS ($\mathbf{F}_\mathrm{k}$):

$$\mathbf{k}^{l,r} \sim \mathbf{F}_\mathrm{k}(\mathbf{k} | \mathbf{f}^{l,r}). \qquad (3)$$

Then, we proceed to simulate the porosity, conditioned to $\mathbf{k}^{l,r}$ and the facies, using co-DSS ($\mathbf{F}_\phi$),

$$\boldsymbol{\phi}^{l,r} \sim \mathbf{F}_\phi(\boldsymbol{\phi} | \mathbf{k}^{l,r}, \mathbf{f}^{l,r}). \qquad (4)$$

Finally, we simulate the acoustic impedance, conditioned to $\boldsymbol{\phi}^{l,r}$, using co-DSS ($\mathbf{F}_{\mathrm{I_P}}$),

$$\mathbf{I_P}^{l,r} \sim \mathbf{F}_{\mathrm{I_P}}(\mathbf{I_P} | \boldsymbol{\phi}^{l,r}, \mathbf{f}^{l,r}). \qquad (5)$$

The sequential simulation approach ensures the reproduction of the marginal and conditional probability distributions of the petroelastic properties in each facies.

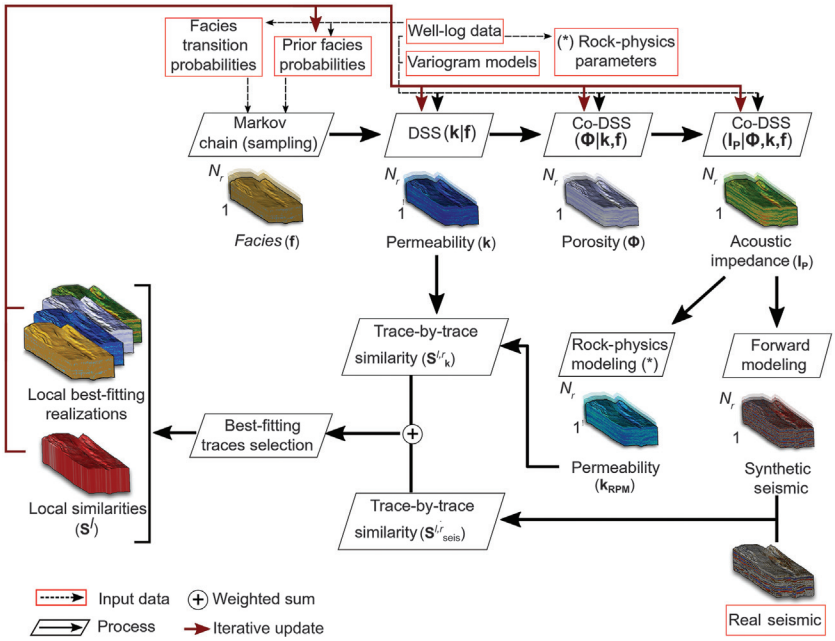


Figure 1. Schematic representation of the proposed iterative geostatistical seismic inversion algorithm.

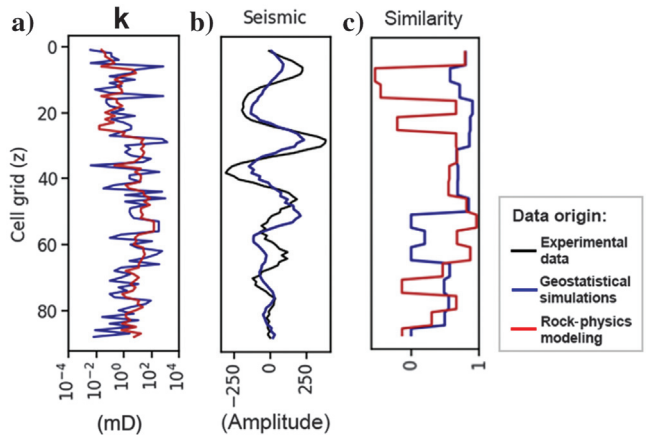


Figure 2. One-dimensional example of (a) stochastic and estimated (rock physics) permeability models, (b) estimated synthetic seismic and observed real seismic trace, and (c) similarity curves calculated comparing permeability models (the red) and seismic data (the blue). The latter is used in the objective function for model perturbation.

## Seismic model

The simulated elastic models of acoustic impedance are used to calculate the seismic reflectivity coefficients series (Russell, 1988) as

$$\mathbf{r}(i) = \frac{\mathbf{I_P}_{i+1} - \mathbf{I_P}_i}{\mathbf{I_P}_{i+1} + \mathbf{I_P}_i}, \tag{6}$$

where $\mathbf{r}(i)$ is the reflection coefficient at the boundary between the layer $i$ and the layer below $i+1$. These models are then convolved with a wavelet to calculate a set of synthetic seismic models. The mismatch between synthetic and real data is defined by a similarity coefficient $\mathbf{S}$ as

$$\mathbf{S}^{l,r}_{\text{seis}} = \frac{2\sum_{s=1}^{N}\mathbf{x}_s\mathbf{y}_s}{\sum_{s=1}^{N}(\mathbf{x}_s) + \sum_{s=1}^{N}(\mathbf{y}_s)}, \tag{7}$$

where the superscript $l$ and $r$ represent the current iteration and realization, respectively; $N$ corresponds to the number of samples; and $\mathbf{x}$ and $\mathbf{y}$ correspond to the predicted and real seismic data, respectively. This similarity coefficient ranges between $-1$ and 1, but all negative coefficients are truncated at zero. Only the positive coefficients are used as part of the objective function for the iterative optimization of the models as positive values maximized the similarity (Figures 1, 2b, and 2c).

## Rock-physics modeling

In the proposed seismic inversion algorithm, a facies-dependent calibrated RPM is used to calculate the expected permeability values given the acoustic impedance model $\mathbf{I}^{l,r}_{\mathbf{P}}$. The calibration of the RPM is based on the available petroelastic well-log data. For example, porosity $\boldsymbol{\phi}$ can be estimated by means of a linear regression from $\mathbf{I_P}$, in the form of $\boldsymbol{\phi} = \beta_1\mathbf{I_P} + \beta_0$, where $\beta_1$ and $\beta_0$ are, respectively, the slope and intercept of the regression. The relation between permeability $\mathbf{k}$ and porosity $\boldsymbol{\phi}$ can be modeled by one of the available petrophysical equations presented in the literature such as the Kozeny-Carman or RPGZ models (e.g., Mavko and Nur, 1997; Glover et al., 2006; Mavko et al., 2019). These models generally depend on the pore geometry, the grain size, and the cementation. In this work, we adopt the RPGZ equation (Glover et al., 2006):

$$k = \frac{d^2\phi^{3m}}{4am^2}, \tag{8}$$

where $d$ is the grain diameter, $a$ is a geometric factor, and $m$ is the cementation exponent.

For each iteration, we calculate a set of permeability models ($\mathbf{k_{rpm}}$) and compute the similarity coefficient $\mathbf{S}_{\text{k}}$ between the permeability trace predicted with rock-physics modeling and predicted from the geostatistical simulation:

$$\mathbf{S}^{l,r}_{k} = \frac{2\sum_{s=1}^{N}\mathbf{u}_s\mathbf{v}_s}{\sum_{s=1}^{N}(\mathbf{u}_s) + \sum_{s=1}^{N}(\mathbf{v}_s)}, \tag{9}$$

where the superscript $l$ and $r$ represent the current iteration and realization, respectively; $N$ corresponds to the number of samples; and $\mathbf{u}$ and $\mathbf{v}$ correspond to the physics constrained models and the geostatistically simulated models of permeability. Similar to the case of the similarity $\mathbf{S}_{\text{seis}}$, negative values of $\mathbf{S}_{\text{k}}$ are truncated to zero. The proposed algorithm combines the similarity $\mathbf{S}_{\text{seis}}$ with the similarity $\mathbf{S}_{\text{k}}$ in the optimization objective function (Figures 1, 2a, and 2c).

## Stochastic update

The optimization function used for the iterative update of the models is defined as the weighted sum:

$$\mathbf{S}^{l,r} = (1 - 0.5\alpha)\mathbf{S}^{l,r}_{\text{seis}} + 0.5\alpha\mathbf{S}^{l,r}_{\text{k}}, \tag{10}$$

where $\mathbf{S}^{l,r}_{\text{seis}}$ is the similarity between real and synthetic seismic (equation 7) and $\mathbf{S}^{l,r}_{\text{k}}$ is the similarity between the stochastic and the rock-physics estimated permeability models (equation 9). The weight $\alpha$ represents the accuracy of the RPM predictions. In the proposed algorithm, $\alpha$ is estimated using the Pearson's coefficient calculated between the permeability logs and the rock-physics predictions of permeability at the well locations. The fixed value 0.5 is used to equally balance the two components of the sum.

At each iteration $l$, facies and petroelastic models with the highest $\mathbf{S}^{l,r}$ are kept for the following iteration as auxiliary variables $(\mathbf{f}^l_{\text{aux}}, \mathbf{k}^l_{\text{aux}}, \boldsymbol{\phi}^l_{\text{aux}}, \mathbf{I}^l_{\mathbf{P}_{\text{aux}}})$ together with their similarity coefficient $\mathbf{S}^l$. The auxiliary variable for the facies models is used to define an indicator variable $i(\mathbf{f}^l)$ (i.e., a binary variable equal to one or zero according to the presence or absence of a facies at a given location). At the following iteration $(l+1)$, a proposal distribution $P(\mathbf{f}^{l+1}|\mathbf{d})$ is obtained by linearly deforming the prior distribution $P(\mathbf{f}^l)$, weighted by the similarity $\mathbf{S}^l$:

$$P(\mathbf{f}^{l+1}|\mathbf{d}) = \mathbf{S}^l i(\mathbf{f}^j) + (1 - \mathbf{S}^l)P(\mathbf{f}^l), \tag{11}$$

according to the probability perturbation method proposed by Caers and Hoffman (2006).

The facies likelihood $P$ conditioned to $\mathbf{S}^l$ data is hence given by

$$P(\mathbf{f}^{l+1}_t|\mathbf{d}, \mathbf{f}^l_{1,\ldots,t-1}) \propto \prod_{z=1}^{t} P(\mathbf{f}_z|\mathbf{f}_{z-1})P(\mathbf{f}^{l+1}|\mathbf{d}), \tag{12}$$

where $t$ is the time sample in the vertical direction and $P(\mathbf{f}_z|\mathbf{f}_{z-1})$ is given by the transition matrix of equation 2 as in Azevedo et al. (2020a).

We then cosimulate sequentially $N_r$ sets of petroelastic properties, locally conditioned to the simulated facies models and the auxiliary variables of the corresponding properties $(\mathbf{k}^l_{\text{aux}}, \boldsymbol{\phi}^l_{\text{aux}}, \mathbf{I}^l_{\mathbf{P}_{\text{aux}}})$ and $\mathbf{S}^l$ from the previous iteration:

$$\mathbf{k}^{l+1,r} \sim \mathbf{F}_{\text{k}}(\mathbf{k}|\mathbf{f}^{l+1,r}, \mathbf{k}^l_{\text{aux}}, \mathbf{S}^l), \tag{13}$$

$$\boldsymbol{\phi}^{l+1,r} \sim \mathbf{F}_{\phi}(\boldsymbol{\phi}|\mathbf{k}^{l+1,r}, \mathbf{f}^{l+1,r}, \boldsymbol{\phi}^l_{\text{aux}}, \mathbf{S}^l), \tag{14}$$

$$\mathbf{I}^{l+1,r}_{\mathbf{P}} \sim \mathbf{F}_{\mathbf{I}_{\text{P}}}(\mathbf{I_P}|\boldsymbol{\phi}^{l+1,r}, \mathbf{f}^{l+1,r}, \mathbf{I}^l_{\mathbf{P}_{\text{aux}}}, \mathbf{S}^l). \tag{15}$$

The variability of the new set of realizations depends on the local coefficient $\mathbf{S}^l$ (Azevedo and Soares, 2017). If $\mathbf{S}$ is high, the geostat-

istical cosimulations realizations will have a low variability within the new ensemble of models. If **S** is low, the geostatistical cosimulations realizations will have high variability within the new ensemble of models. The spatial continuity pattern of the new set of models depends on the imposed variogram model used in the stochastic sequential cosimulation and the transition matrix used in the first-order Markov Chain.

## APPLICATION EXAMPLES

To illustrate the proposed seismic inversion algorithm for permeability prediction, we applied it to a 1D synthetic example and to a real data set including a 3D full-stack seismic volume with scarce well-log data. In both study cases, we run a seismic inversion for the characterization of a carbonate geologic sequence. The data used were measured on a carbonate sequence of the Albian age, in the Brazilian offshore. Using the available geologic knowledge and petrophysical data, we classified the lithologies into two main facies (**f**): facies 1 is a well-cemented packstone, with low porosity (up to 10%) and relatively lower permeability (up to 100 mD) and facies 2 is a calcarenite, with higher porosity (8%–19%) and permeability (1–350 mD). This facies classification is used for synthetic and real case studies.

### Synthetic case study

We first validated the proposed method on a synthetic seismogram inspired by real well-log data. The data set includes a time window of 77 samples. The synthetic seismic trace is calculated as the convolution of the $\mathbf{I_P}$ well log using a wavelet extracted from the real full-stack seismic volume (Figure 3a). In this example, we do not account for the uncertainty associated with the seismic-to-well tie, wavelet estimation, and forward model approximation.

We calibrated a facies-dependent RPM using the well-log data, as shown in Figure 3a and 3b. The parameters of the RPM are shown in Table 1. The value of the accuracy parameter $\alpha$ of the RPM (equation 10), calculated as the correlation of the real and predicted permeability logs, is 0.89. We also calculated a transition matrix (Table 2) from the reference log profile (Figure 3a) and vertical variogram models fitted to the experimental variograms computed from the true logs. The variogram models have a zero nugget and range of 15, 14.5, and 13 ms for permeability, porosity, and impedance, respectively.

We ran the proposed geostatistical inversion with rock-physics constraints and compared its results with those obtained with a traditional geostatistical inversion (Azevedo et al., 2020a). Both methods generated 32 realizations of facies and petroelastic properties per iteration, running for a total of six iterations. The simulations are conditioned at three vertical locations of the borehole (green-filled circles in Figure 3a), used as experimental samples. The model realizations exactly match the values at the location of the experimental data, whereas, at all of the other locations, they reproduce the facies transition matrix, the marginal and joint distributions of the continuous properties, and the vertical variogram.

The results obtained after the first iteration from both methods are shown in Figures 4 and 5. Both inversion techniques provide similar results, by construction, and the joint distribution of permeability and porosity reproduces the experimental ones observed at the well location in each facies (Figure 4c). After six iterations, the models generated by both algorithms match the ground truth (Figures 6 and 7).

The traditional geostatistical approach inversion shows a significant overestimation of the facies 1 proportion, permeability and porosity, and an underestimation of impedance. The results obtained with the proposed method show higher prediction accuracy, as shown by the most likely facies model resulting from the last realizations (Figure 6b). Analogously, the permeability models are closer to the real well log (Figure 6a). The uncertainty predicted from the proposed method (i.e., the P10–P90 interval defined by the 10th and 90th percentiles of the set of simulated models) better represents the variability of the continuous properties. Figures 6a and 7 show the percentage of well-log samples that are within the predicted P10 and P90 curves. Despite an improvement in the prediction of the continuous variables, the seismic data mismatch (Figure 7a and 7b) of the proposed inversion shows a worse fit with the true seismic trace, possibly due to the rock-physics constraint in the objective function.

### Real case study

We then applied the proposed inversion to a real case study, including 3D seismic reflection data acquired over the area that extends along 13.25 km in the north–south direction and 7.60 km in the east–west direction (Figure 8). The inversion interval is approximately 250 ms two-way traveltime (TWT). Well-log data are available at four

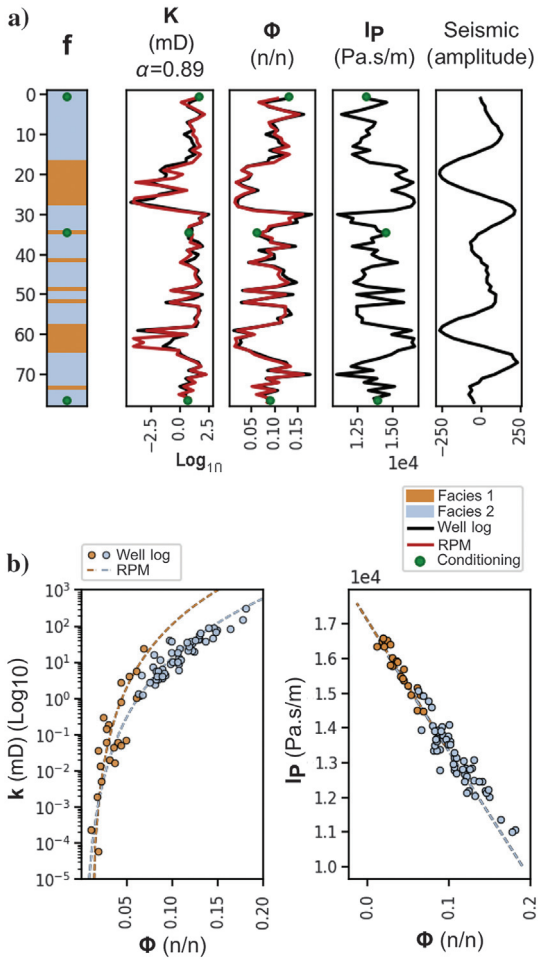


Figure 3. One-dimensional synthetic data set: (a) facies log (**f**), real well logs and calibrated RPM predictions, and conditioning data and (b) joint distributions retrieved from well-log data and RPMs.

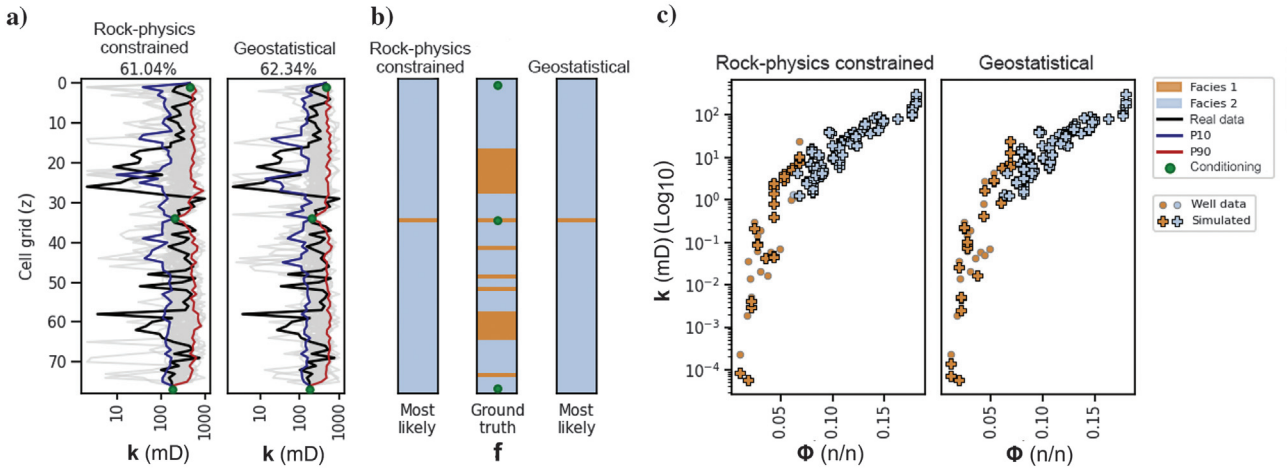


Figure 4. Permeability (**k**) and facies (**f**) models resulting from the first iteration of the synthetic study case for geostatistical with and without rock-physics constraints: (a) **k** simulations and well log, (b) **f** most likely facies models and well log, and (c) **k** versus $\phi$ joint distributions for a single realization.

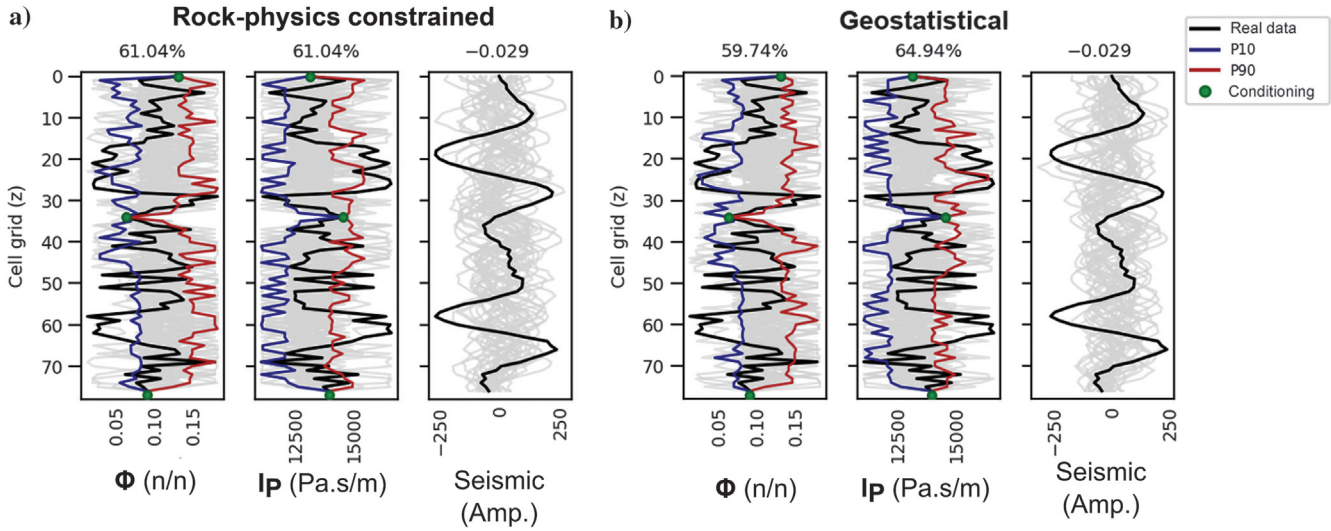


Figure 5. Simulations of $\phi$, $\mathbf{I_P}$, and corresponding synthetic seismic data resulting from the first iteration: (a) rock-physics constrained and (b) geostatistical inversion. Percentage values indicate the percentage of well-log data included between the P10 and P90 curves; an average $\mathbf{S}_{seis}$ from all of the realizations is shown for the seismic traces.

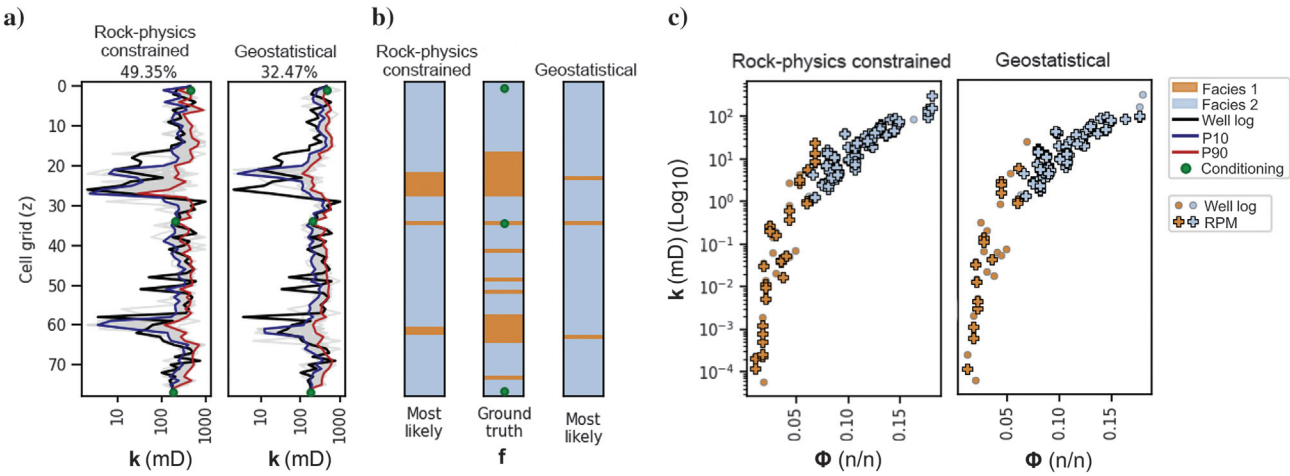


Figure 6. Permeability and facies models resulting from the sixth iteration of the synthetic study case for geostatistical with and without rock-physics constrains: (a) **k** simulations, (b) facies models, and (c) **k**–$\boldsymbol{\phi}$ joint distributions for a single realization.

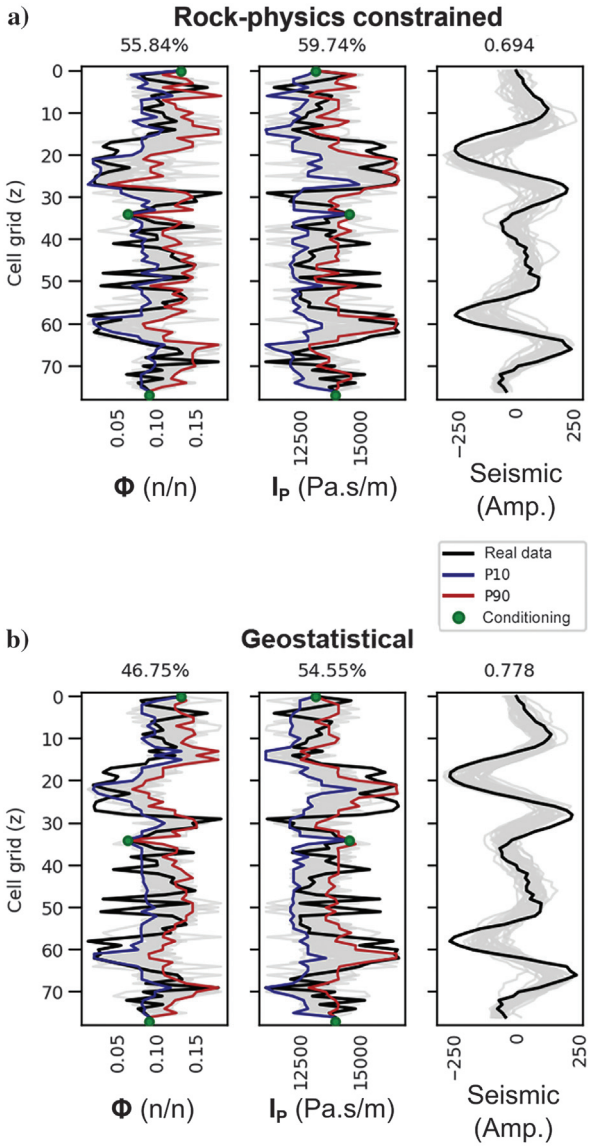


Figure 7. Simulations of $\boldsymbol{\phi}$, $\mathbf{I_P}$, and corresponding synthetic seismic data resulting from the sixth iteration: (a) rock-physics constrained and (b) geostatistical inversion. Percentage values indicate the percentage of well-log data included between the P10 and P90 curves; an average $\mathbf{S}_{\text{seis}}$ from all of the realizations is shown for the seismic traces.

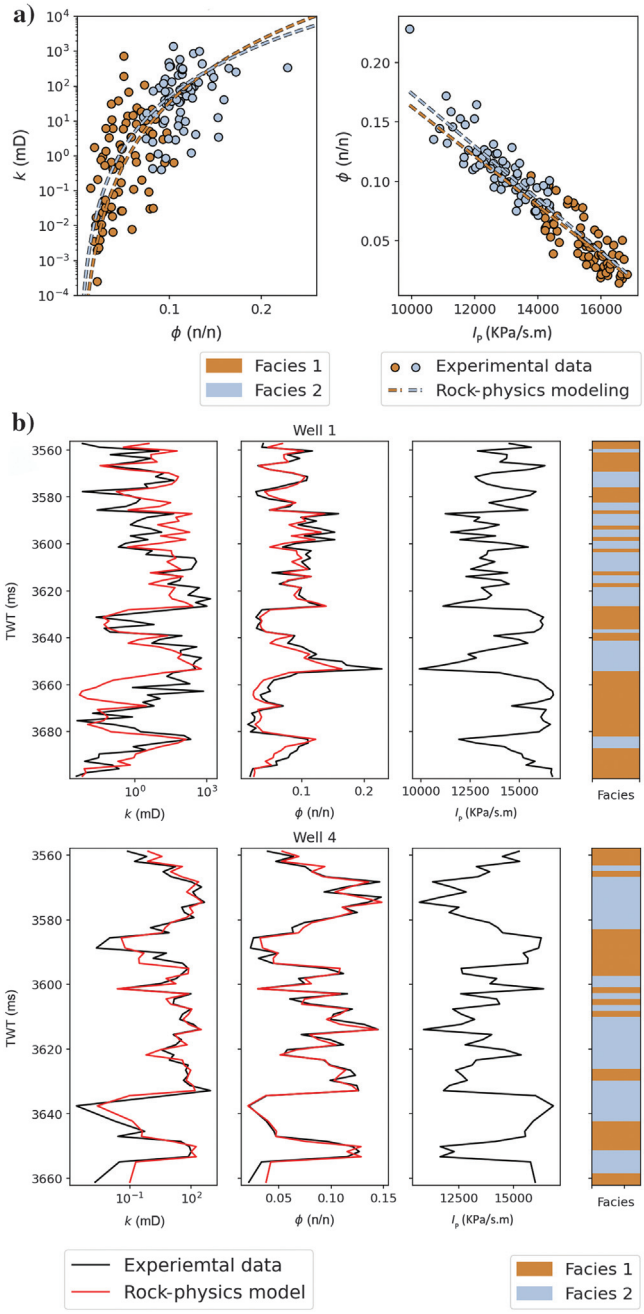


Figure 9. Well-log data and RPM calibration from the real case application. (a) Joint experimental distributions and (b) real logs and rock-physics predictions.

Figure 8. (a) Seismic grid and relative location of well data used for the real case application. Well W2 (the blue) does not have **k** log; well W3 (the red) was used to assess locally the performance of the proposed inversion method. The red line represents the vertical well section used to illustrate the results. (b) Recorded full-stack seismic reflection data.

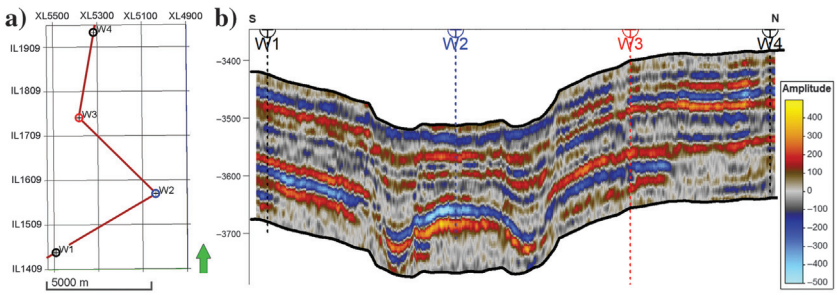

**Table 1. Parameters used for the RPM for the synthetic case.**

| Porosity-permeability | Facies 1 | Facies 2 |
|---|---|---|
| $d$ (mm) | 0.7 | 0.35 |
| $m$ | 1.9 | 1.8 |
| $a$ | 2/3 | 10/3 |
| Impedance-porosity | | |
| $\beta_1$ (m/s g/cm$^3$)$^{-1}$ | −2.36e−5 | −2.81e−5 |
| $\beta_0$ | 0.41 | 0.48 |

Parameters and equations are defined in the rock-physics modeling section.

well locations (Figure 8) and include $\mathbf{f}$, $\boldsymbol{\phi}$, $\mathbf{k}$ (except for well W2), and $\mathbf{I_P}$. Well W3 is used as a blind-well test, whereas the other three wells are used for data conditioning and model calibration.

For the geostatistical simulations and cosimulations, we imposed 3D variogram models fitted to the observed data. For the horizontal direction, the variogram was modeled from the experimental variogram computed from the observed seismic amplitude. The vertical variogram model was fitted to an experimental variogram computed from the well logs. The variogram models are represented by a nested structure of two exponential models with weights 0.68 and 0.32, with zero nugget. The correlation lengths are shown in Table 3.

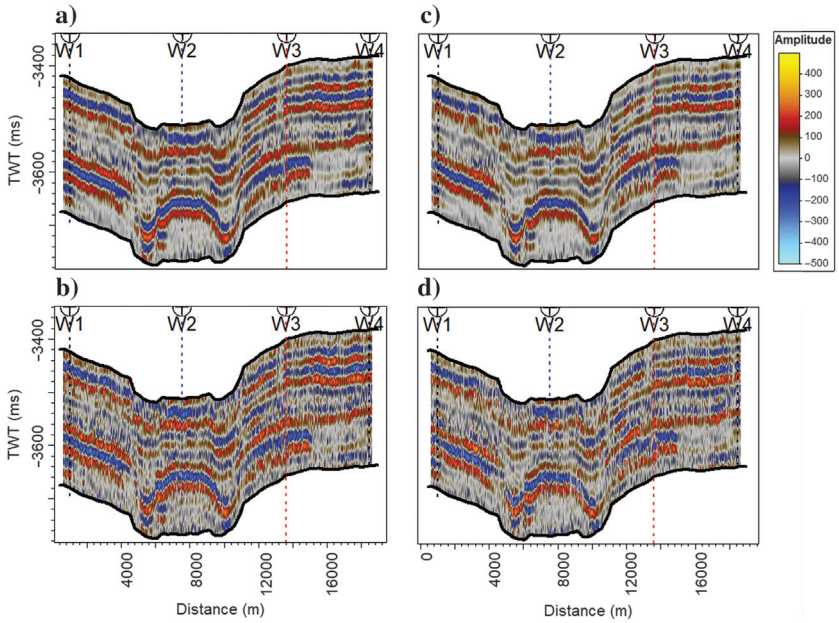


Figure 10. Synthetic seismic volumes calculated at the last iteration from (a) the pointwise average of 32 $\mathbf{I_P}$ models from the proposed inversion method, (b) the best-fit $\mathbf{I_P}$ model out of the 32 models from the proposed method, and (c and d) corresponding models resulting from the geostatistical method.

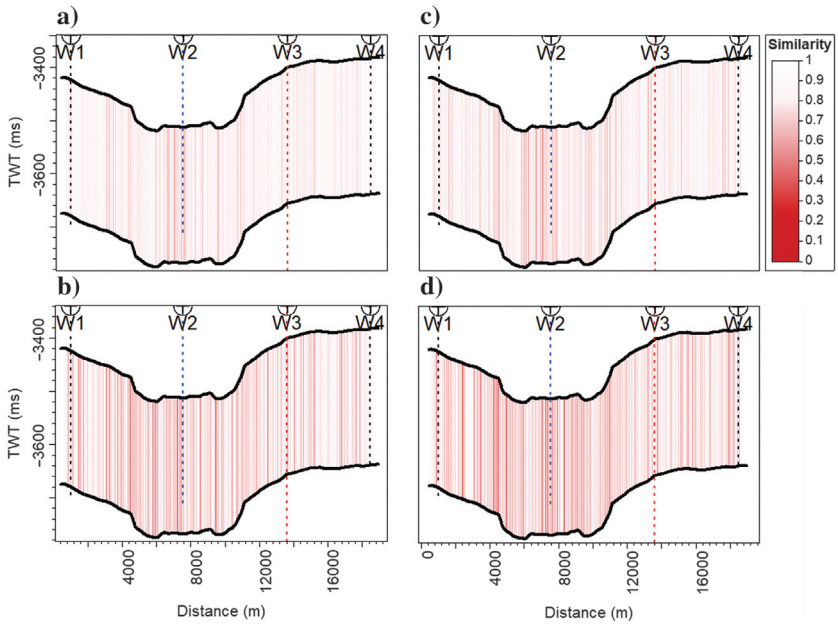


Figure 11. Trace-by-trace seismic data similarity ($\mathbf{S_{seis}}$) between the real seismic data (Figure 8) and the synthetic seismic models shown in Figure 10: (a) average model from the proposed method, (b) best-fit model from the proposed inversion, and (c and d) corresponding models obtained from the geostatistical method.

The facies transition matrix is estimated from the log-facies profiles at the well locations, whereas the RPM parameters are fitted to the well logs (Table 4 and Figure 9). The objective function weight parameter $\alpha$ is calculated to be 0.75; this represents the average accuracy value calculated on the rock-physics predictions of $\mathbf{k}$ at wells W1 and W2 (Figure 9b).

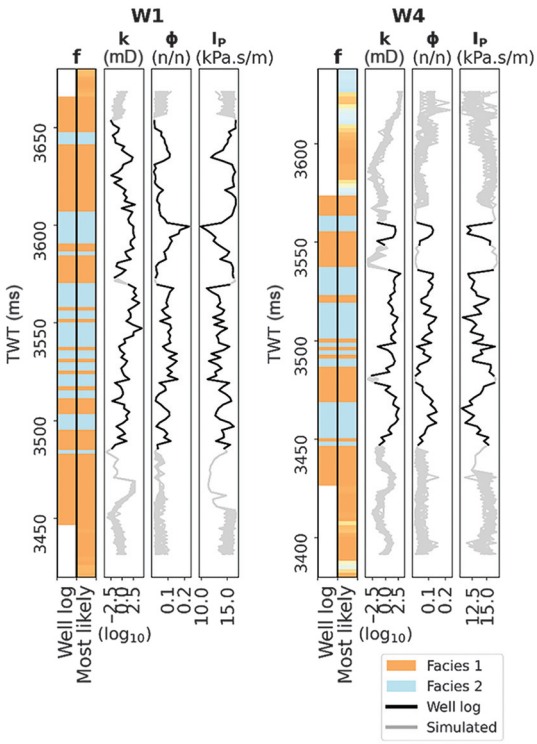


Figure 12. Comparison of the well-log data from wells W1 and W4 with the most likely facies models and the ensemble of 32 realizations obtained from the last iteration of the proposed method. Facies and petroelastic models honor the conditioning experimental data.

We ran the proposed seismic inversion method with six iterations, generating 32 facies and petroelastic models per iteration. The results are compared with those predicted from the standard geostatistical seismic inversion method (Azevedo et al., 2020a). Both methods converge toward solutions that reproduce the seismic data, including their spatial continuity and amplitude content (Figure 10). The trace-by-trace similarity between the predicted and the observed seismic data is shown in Figure 11. Overall, the proposed method (Figure 10a and 10b) produced results that are closer to the observed seismic data: the average $\mathbf{S}_{\text{sies}}$ for the proposed method is 0.77 (standard deviation $3.1 \times 10^{-4}$) whereas, for the geostatistical method, the result is 0.75 (standard deviation $2.9 \times 10^{-4}$). The location of poor convergence shown in Figure 11 corresponds to more uncertain areas due to the poor signal-to-noise ratio of the observed seismic data or the nonstationary nature of the wavelet.

The predicted facies and petroelastic realizations obtained with the Markov chain and DSS and co-DSS honor the experimental data (Figure 12). The facies models at the last iteration are summarized in Figure 13 and include the likelihood of facies 1 (Figure 13a and 13c) and the most likely facies model (Figure 13b and 13d). The predictions (Figure 13a and 13b) show a larger lateral continuity than the standard geostatistical method (Figure 13c and 13d). In addition, the proposed method detects thin and laterally continuous layers of facies 2 that are undetected or poorly reproduced by the

**Table 2. Transition matrix of the facies profile for the synthetic case.**

| | Facies 1 | Facies 2 |
|---|---|---|
| Facies 1 | 0.85 | 0.15 |
| Facies 2 | 0.07 | 0.93 |

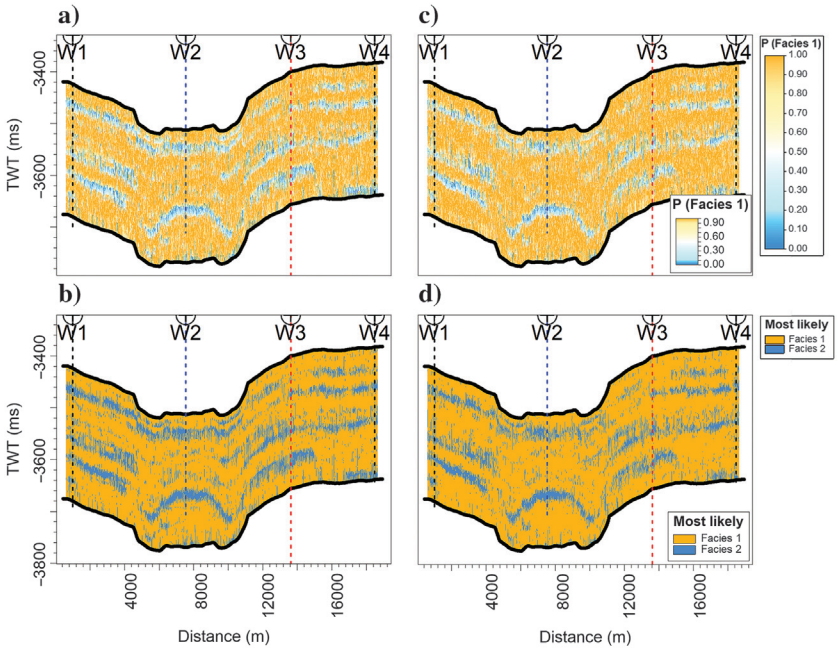


Figure 13. (a) Pointwise likelihood of facies 1, calculated from the ensemble of 32 realizations at the last iteration of the inversion with the proposed inversion method, (b) most likely facies model calculated from the last iteration results of the proposed method, and (c and d) corresponding models resulting from the geostatistical method.

traditional inversion method (Figure 13c and 13d). Such features also are reproduced in the stochastic simulations of permeability (Figure 14a). Compared with the traditional inversion results (Figure 14d), the proposed inversion method predicts thinner permeable layers, corresponding to facies 2 (e.g., between 10 and 12 km of distance, at TWT approximately 3620 ms). The distributions of porosity (Figure 14b) and acoustic impedance (Figure 14c) predicted by the proposed algorithm have a higher vertical and lateral resolution compared with the iterative geostatistical seismic inversion results (Figure 14e and 14f).

The results at the blind-well (W3) location (Figure 15) show the match between the predicted models and real well-log data. The facies sequence is well reproduced by the most likely facies model predicted by the proposed method (Figure 15a). The proposed inversion method captures the facies sequence between 3460 and 3490 ms and the facies intercalations between 3500 and 3550 ms, whereas the traditional inversion method (Figure 15b) predicts a continuous layer of facies 2. The petroelastic properties match the true logs, with local dissimilarities where the facies prediction is uncertain. The permeability experimental data are better reproduced by the proposed method, whereas porosity and acoustic impedance predictions show similar results.

**Table 3. Parameters of the 3D variogram model for the real case.**

| | | Range | | |
|---|---|---|---|---|
| | Structure number | Inline (m) | Crossline (m) | Vertical (ms) |
| **k** | 1 | 54 | 44 | 7.5 |
| | 2 | 500 | 240 | 7.5 |
| **ϕ** | 1 | 54 | 44 | 7.25 |
| | 2 | 500 | 240 | 7.25 |
| $\mathbf{I_P}$ | 1 | 54 | 44 | 6.5 |
| | 2 | 500 | 240 | 6.5 |

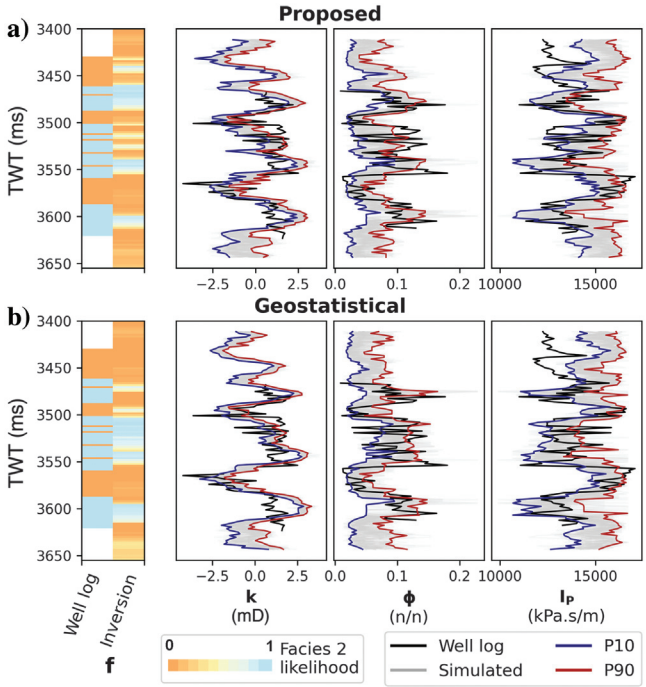


Figure 15. Results from the last iteration at the blind well location (W4) compared with the colocated well-log data: (a) results from using the proposed inversion method and (b) results using the geostatistical inversion method.

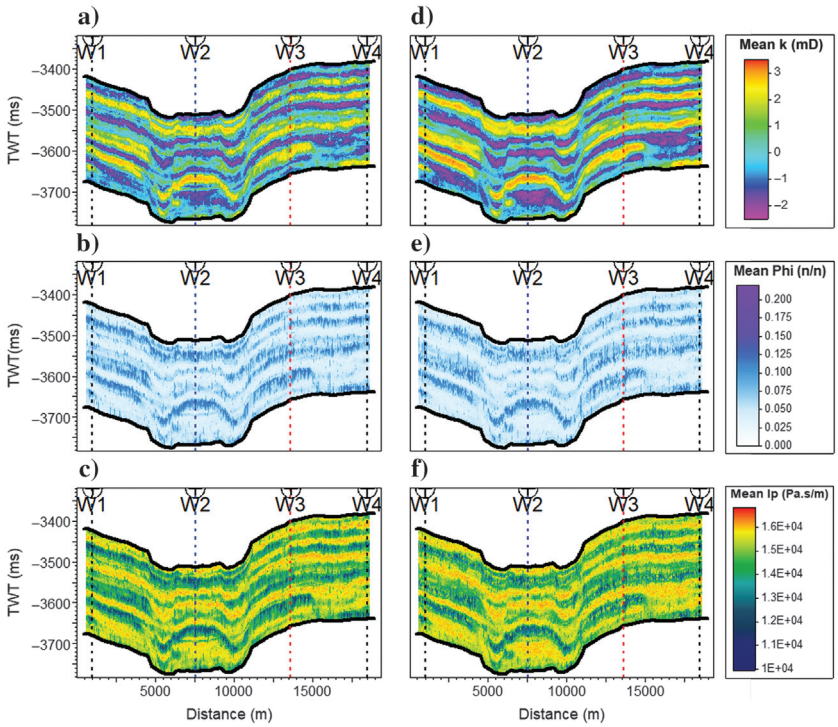


Figure 14. A pointwise average calculated from the ensemble of 32 realizations at the last iteration of the inversion using the proposed inversion method, respectively, for (a) **k**, (b) **ϕ**, and (c) $\mathbf{I_P}$. The same models are shown for the geostatistical methods, for (d) **k**, (e) **ϕ**, and (f) $\mathbf{I_P}$.

## DISCUSSION

The proposed iterative geostatistical seismic inversion algorithm aims to predict subsurface permeability models by accounting for the rock-physics prior information. We applied this methodology to synthetic and real data and compared it to an iterative geostatistical seismic inversion method in which no prior rock-physics information is used in the model update. Considering the two application examples, we show how including rock-physics constraints in the geostatistical seismic inversion improves the predicted models and imposes physical constraints on the solution. The results are accurate when tested on a blind-well test (Figures 6 and 15) and show improved spatial continuity of the predicted facies and petroelastic models (Figures 13 and 14). In the real study case, the variance of permeability is larger than the traditional method (Figure 16a and 16d), whereas it is similar for other properties. This effect demonstrates the ability of the proposed method to better explore the model parameter space, especially for permeability.

**Table 4. Parameters of the RPM for the real case.**

| Porosity-permeability | Facies 1 | Facies 2 |
|---|---|---|
| $d$ (mm) | 0.6 | 0.4 |
| $m$ | 2 | 1.65 |
| $a$ | 2/3 | 10/3 |
| Impedance-porosity | | |
| $\beta_1$ (m/s g/cm$^3$)$^{-1}$ | −2.08e−5 | −2.22e−5 |
| $\beta_0$ | 0.37 | 0.39 |

The choice of an RPM mostly depends on the study case. Here, we adopted the RGPZ model (Glover et al., 2006), whose parameters are related to the rock texture and cementation. These parameters were inferred from the thin sections and samples. The integration of the RPM in geostatistical inversion is challenging to the lateral correlation in the subsurface. The secondary set of permeability models estimated from acoustic impedance using the RPM does not account for the spatial patterns of the geologic model but imposes a physical constraint in the objective function of the stochastic optimization. The iteratively updated set of solutions is coherent with the RPM, the observed data, and their spatial structure. The weight of the rock-physics constraints is effective proportionally to the quality of the RPM parameterization. A poorly informed RPM would have less weight in the iterative process.

The facies classification is embedded in the inversion through the stochastic simulation and updating of a 1D Markov chain. The method is illustrated for two facies but can be extended to any finite number of facies, using the indicator variables, as long as they can be discriminated at the seismic scale. In theory, the method also could be extended to 2D and 3D Markov models to avoid lateral discontinuities; however, the computational cost of such methods is much larger, and the simulation might not honor the geometry of the geologic horizons. Despite the use of a vertical model only, the horizontal continuity of the facies is fairly reproduced during the simulation/cosimulation of the continuous properties, which conditions the facies generation and ensures horizontal continuity at the following iteration.

The proposed algorithm is here described and tested for the inversion of poststack seismic data. However, it can be extended to the inversion of pre- or partial-stack seismic data if a suitable poroelastic model is available, accordingly to the study case. The following paragraph describes each algorithm step in more detail.

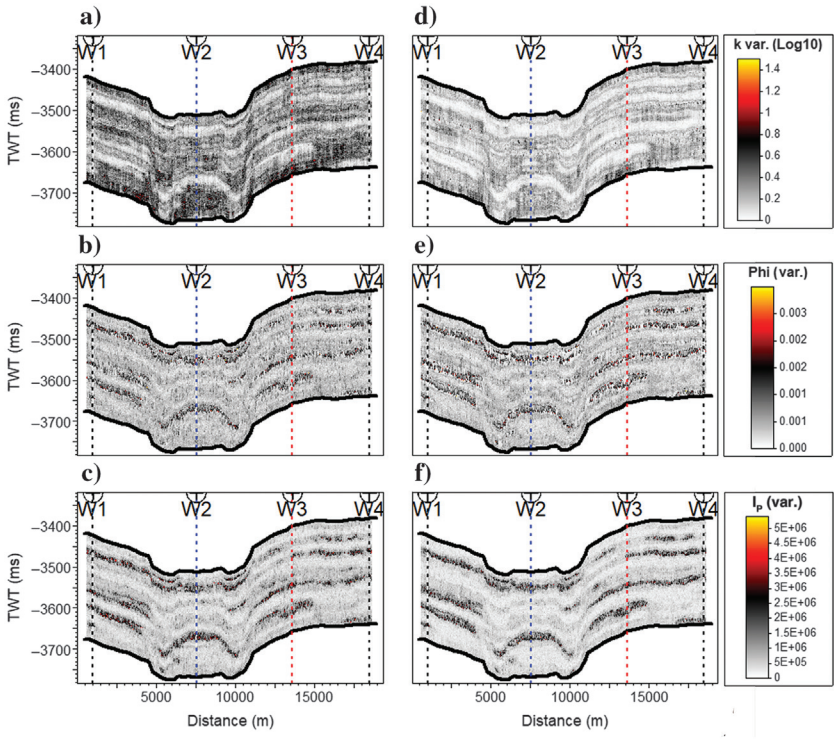


Figure 16. The pointwise variance of the realizations generated at the last iteration of **k**, **ϕ**, and $\mathbf{I_P}$, using the proposed method (respectively, [a–c]) and the traditional geostatistical method (respectively, [d–f]).

## CONCLUSION

The proposed iterative geostatistical seismic method predicts the spatial distribution of permeability using rock-physics constraints, rather than uniquely relying on the reproduction of the experimental joint distributions of petroelastic properties. In a geostatistical approach, acoustic impedance is cosimulated from permeability: there is not an explicit model, but only a statistical correlation inferred from well-log data. We then calculate a permeability spatial distribution from acoustic impedance using a model based on rock physics (priorly known). Comparing the two aims at penalizing the geostatistical realizations that are not reliable from a "rock physics perspective." This form *cycle consistency* gives us the constraints necessary to link permeability distributions to the corresponding seismic amplitudes. This approach is especially valuable for applications with limited well-log data, where it is challenging to estimate the joint distribution. The simulation of the model variables is based on

geostatistical algorithms, whereas the optimization is based on an objective function that depends on a trade-off between seismic mismatch and rock-physics constraints. The method is validated on two case studies using synthetic and real data. For both, we showed a comparison with a traditional geostatistical inversion based on the seismic data misfit. The comparison shows that the rock-physics constraints improve the results of a seismic inversion in realistic noise conditions. The proposed method allows for overcoming the weak correlation between permeability spatial distribution and seismic reflection data. The proposed inversion is computationally efficient and can be applied to various geologic environments as long as an RPM is available.

## ACKNOWLEDGMENTS

The authors want to express their gratitude to FCT - Fundação para a Ciência e a Tecnologia (Reference 2020.05571.BD), for funding this project. R. Miele, D. Grana, and L. Azevedo would like to thank Petrobras for providing the data and the permission to publish it, as well as Schlumberger, France, for the donation of academic licenses of Petrel software.

## DATA AND MATERIALS AVAILABILITY

Data associated with this research are available and can be obtained by contacting the corresponding author.

## REFERENCES

Avseth, P., T. Mukerji, and G. Mavko, 2005, Quantitative seismic interpretation: Cambridge University Press.
Azevedo, L., D. Grana, and C. Amaro, 2019, Geostatistical rock physics AVA inversion: Geophysics Journal International, **216**, 1728–1739, doi: 10.1093/gji/ggy511.
Azevedo, L., D. Grana, and L. de Figueiredo, 2020a, Stochastic perturbation optimization for discrete-continuous inverse problems: Geophysics, **85**, no. 5, M73–M83, doi: 10.1190/geo2019-0520.1.
Azevedo, L., J. Narciso, R. Nunes, and A. Soares, 2020b, Geostatistical seismic inversion with self-updating of local probability distributions: Mathematical Geosciences, **53**, 1073–1093, doi: 10.1007/s11004-020-09896-9.
Azevedo, L., and A. Soares, 2017, Geostatistical methods for reservoir geophysics: Springer International Publishing.
Biot, M. A., 1956a, Theory of propagation of elastic waves in a fluid-saturated porous solid. I. Low-frequency range: The Journal of the Acoustical Society of America, **28**, 168–178, doi: 10.1121/1.1908239.
Biot, M. A., 1956b, Theory of propagation of elastic waves in a fluid-saturated porous solid. II. Higher frequency range: The Journal of the Acoustical Society of America, **28**, 179–191, doi: 10.1121/1.1908241.
Bosch, M., T. Mukerji, and E. F. Gonzalez, 2010, Seismic inversion for reservoir properties combining statistical rock physics and geostatistics: A review: Geophysics, **75**, no. 5, 75A165–75A176, doi: 10.1190/1.3478209.
Buland, A., and H. Omre, 2003, Bayesian linearized AVO inversion: Geophysics, **68**, 185–198, doi: 10.1190/1.1543206.
Butler, J. J., 2005, Hydrogeological methods for estimation of spatial variations in hydraulic conductivity, *in* Y. Rubin and S. S. Hubbard, eds., Hydrogeophysics. Water science and technology library: Springer, **50**, 23–58.
Caers, J., and T. Hoffman, 2006, The probability perturbation method: A new look at Bayesian inverse modeling: Mathematical Geology, **38**, 81–100, doi: 10.1007/s11004-005-9005-9.
Carcione, J. M., 2015, Wave fields in real media: Wave propagation in anisotropic, anelastic, porous and electromagnetic media: Elsevier.
Carman, P. C., 1937, Fluid flow through granular beds: Transactions of the Institution of Chemical Engineers, **15**, 150–166.
Coates, G. R., L. Xiao, and P. Manfred, 1999, Logging principles and applications: Haliburton Energy Services, 234.
Dadashpour, M., 2009, Reservoir characterization using production data and time-lapse seismic data: Doctoral dissertation, Norwegian University of Science and Technology (NTNU).
Dadashpour, M., D. Echeveria Ciaurri, T. Mukerji, J. Kleppe, and M. Landrø, 2010, A derivative-free approach for the estimation of porosity and permeability using time-lapse seismic and production data: Journal of Geophysics and Engineering, **7**, 351.
de Figueiredo, L. P., D. Grana, F. L. Bordignon, M. Santos, M. Roisenberg, and B. B. Rodrigues, 2018, Joint Bayesian inversion based on rock-physics prior modeling for the estimation of spatially correlated reservoir properties: Geophysics, **83**, no. 5, M49–M61, doi: 10.1190/geo2017-0463.1.
Deutsch, C. V., 2002, Geostatistical reservoir modeling: Oxford University Press.
Deutsch, C. V., and A. G. Journel, 1997, GSLIB: Geostatistical software library and user's guide: Oxford University Press.
Doyen, P., 2007, Seismic reservoir characterization: An earth modelling perspective: EAGE.
Dubrule, O., 2003, Geostatistics for seismic data integration in earth models: SEG and EAGE.
Dunn, K.-J., D. J. Bergman, and G. A. Latorraca, 2002, Nuclear magnetic resonance petrophysical and logging applications: Pergamon.
Dvorkin, J., M. Gutierrez, and D. Grana, 2014, Seismic reflections of rock properties: Cambridge University Press.
Dvorkin, J., R. Nolen-Hoeksema, and A. Nur, 1994, The squirt-flow mechanism: Macroscopic description: Geophysics, **59**, 428–438, doi: 10.1190/1.1443605.
Elfeki, A., and M. Dekking, 2001, A Markov chain model for subsurface characterization: Theory and applications: Mathematical Geology, **33**, 569–589, doi: 10.1023/A:1011044812133.
Ellis, D. V., and J. M. Singer, 2007, Well logging for earth scientists, 2nd ed.: Springer.
Feng, T., and T. Mannseth, 2010, Impact of time-lapse seismic data for permeability estimation: Computational Geosciences, **14**, 705–719, doi: 10.1007/s10596-010-9182-6.
Fjeldstad, T., and H. Omre, 2020, Bayesian inversion of convolved hidden Markov models with applications in reservoir prediction: IEEE Transactions on Geoscience and Remote Sensing, **58**, 1957–1968, doi: 10.1109/TGRS.2019.2951205.
Glover, P. W., I. I. Zadjali, and K. A. Frew, 2006, Permeability prediction from MICP and NMR data using an electrokinetic approach: Geophysics, **71**, no. 4, F49–F60, doi: 10.1190/1.2216930.
Goloshubin, G., D. Silin, V. Vingalov, G. Takkand, and M. Latfullin, 2008, Reservoir permeability from seismic attribute analysis: The Leading Edge, **27**, 376–381, doi: 10.1190/1.2896629.
González, E. F., T. Mukerji, and G. Mavko, 2008, Seismic inversion combining rock physics and multiple-point geostatistics: Geophysics, **73**, no. 1, R11–R21, doi: 10.1190/1.2803748.
Grana, D., and E. Della Rossa, 2010, Probabilistic petrophysical-properties estimation integrating statistical rock physics with seismic inversion: Geophysics, **75**, no. 3, O21–O37, doi: 10.1190/1.3386676.
Grana, D., T. Mukerji, and P. Doyen, 2021, Seismic reservoir modeling: Theory, examples, and algorithms: Wiley Blackwell.
Grana, D., T. Mukerji, J. Dvorkin, and G. Mavko, 2012, Stochastic inversion of facies from seismic data based on sequential simulations and probability perturbation method: Geophysics, **77**, no. 4, M53–M72, doi: 10.1190/geo2011-0417.1.
Horta, A., and A. Soares, 2010, Direct sequential co-simulation with joint probability distributions: Mathematical Geosciences, **42**, 269–292, doi: 10.1007/s11004-010-9265-x.
Iturrarán-Viveros, U., and J. O. Parra, 2014, Artificial neural networks applied to estimate permeability, porosity and intrinsic attenuation using seismic attributes and well-log data: Journal of Applied Geophysics, **107**, 45–54, doi: 10.1016/j.jappgeo.2014.05.010.
Kozeny, J., 1927, Uber kapillare leitung der wasser in boden: Royal Academy of Science, **136**, 271–306.
Krumbein, W. C., and M. F. Dacey, 1969, Markov chains and embedded Markov chains in geology: Journal of the International Association for Mathematical Geology, **1**, 79–96, doi: 10.1007/BF02047072.
Landrø, M., 2001, Discrimination between pressure and fluid saturation changes from time-lapse seismic data: Geophysics, **66**, 836–844, doi: 10.1190/1.1444973.
Lee, M. W., and W. F. Waite, 2008, Estimating pore-space gas hydrate saturations from well log acoustic data: Geochemistry, Geophysics, Geosystems, **9**, doi: 10.1029/2008GC002081.
Lindberg, D. V., and H. Omre, 2015, Inference of the transition matrix in convolved hidden Markov models and the generalized Baum-Welch algorithm: IEEE Transactions on Geoscience and Remote Sensing, **53**, 6443–6456, doi: 10.1109/TGRS.2015.2440415.
Lishman, J. R., 1970, Core permeability anisotropy: Journal of Canadian Petroleum Technology, **9**, doi: 10.2118/70-02-01.
Ma, Y. Z., 2019, Quantitative geosciences: Data analytics, geostatistics, reservoir characterization and modeling: Springer International Publishing.
Mavko, G., T. Mukerji, and J. Dvorkin, 2019, The rock physics handbook, 3rd ed.: Cambridge University Press.
Mavko, G., and A. Nur, 1997, The effect of a percolation threshold in the Kozeny-Carman relation: Geophysics, **62**, 1480–1482, doi: 10.1190/1.1444251.
Nelson, P., 1994, Permeability-porosity relationships in sedimentary rocks: Log Analyst, **35**, 38–62.

Nunes, R., A. Soares, L. Azevedo, and P. Pereira, 2017, Geostatistical seismic inversion with direct sequential simulation and co-simulation with multi-local distribution functions: Mathematical Geosciences, **49**, 583–601, doi: 10.1007/s11004-016-9651-0.

Pride, S. R., J. G. Berryman, and J. M. Harris, 2004, Seismic attenuation due to wave-induced flow: Wave-induced flow losses: Journal of Geophysical Research: Solid Earth, **109**, B01201, doi: 10.1029/2003JB002639.

Pride, S. R., J. M. Harris, D. L. Johnson, A. Mateeva, K. T. Nihel, R. L. Nowack, J. W. Rector, H. Spetzler, R. Wu, T. Yamomoto, J. G. Berryman, and M. Fehler, 2003, Permeability dependence of seismic amplitudes: The Leading Edge, **22**, 518–525, doi: 10.1190/1.1587671.

Rubino, J. G., D. R. Velis, and K. Holliger, 2012, Permeability effects on the seismic response of gas reservoirs: Permeability effects on seismic data: Geophysical Journal International, **189**, 448–468, doi: 10.1111/j.1365-246X.2011.05322.x.

Russell, B. H., 1988, Introduction to seismic inversion methods: SEG.

Shapiro, S. A., and T. Müller, 1999, Seismic signatures of permeability in heterogeneous porous media: Geophysics, **64**, 99–103, doi: 10.1190/1.1444536.

Shepherd, R. G., 1989, Correlations of permeability and grain size: Groundwater, **27**, 633–638, doi: 10.1111/j.1745-6584.1989.tb00476.x.

Silva, F., C. Beneduzi, G. Nassau, and T. Rossi, 2019, Using sonic log to estimate porosity and permeability in carbonates: Proceedings of the 16th International Congress of the Brazilian Geophysical Society & EXPOGEF, 1–5.

Soares, A., 2001, Direct sequential simulation and cosimulation: Mathematical Geology, **33**, 911–926, doi: 10.1023/A:1012246006212.

Soares, A., J. D. Diet, and L. Guerreiro, 2007, Stochastic inversion with a global perturbation method: 69th Annual International Conference and Exhibition, EAGE, Extended Abstracts, doi: 10.3997/2214-4609.201403048.

Tarantola, A., 2005, Inverse problem theory and methods for model parameter estimation: SIAM.

Tiab, D., and E. C. Donaldson, 2012, Petrophysics: Theory and practice of measuring reservoir rock and fluid transport properties, 3rd ed.: Gulf Professional Pub.

Vasco, D. W., A. Datta-Gupta, R. Behrens, P. Condon, and J. Rickett, 2004, Seismic imaging of reservoir flow properties: Time-lapse amplitude changes: Geophysics, **69**, 1425–1442, doi: 10.1190/1.1836817.

White, J. E., N. Mihailova, and F. Lyakhovitsky, 1975, Low-frequency seismic waves in fluid-saturated layered rocks: The Journal of the Acoustical Society of America, **57**, S30–S30, doi: 10.1121/1.1995164.

Yang, S., 2017, Permeability of reservoir rocks, *in* Fundamentals of petrophysics, Springer geophysics: Springer, 233–295, doi: 10.1007/978-3-662-55029-8_6.

Biographies and photographs of the authors are not available.